



**HAL**  
open science

## Microplastics in a salt-wedge estuary: Vertical structure and tidal dynamics

Sophie Defontaine, Damien Sous, Javier Tesan, Mathilde Monperrus,  
Véronique Lenoble, Laurent Lanceleur

### ► To cite this version:

Sophie Defontaine, Damien Sous, Javier Tesan, Mathilde Monperrus, Véronique Lenoble, et al.. Microplastics in a salt-wedge estuary: Vertical structure and tidal dynamics. *Marine Pollution Bulletin*, 2020, 160, pp.111688. 10.1016/j.marpolbul.2020.111688 . hal-02945061

**HAL Id: hal-02945061**

**<https://hal.science/hal-02945061>**

Submitted on 22 Sep 2020

**HAL** is a multi-disciplinary open access archive for the deposit and dissemination of scientific research documents, whether they are published or not. The documents may come from teaching and research institutions in France or abroad, or from public or private research centers.

L'archive ouverte pluridisciplinaire **HAL**, est destinée au dépôt et à la diffusion de documents scientifiques de niveau recherche, publiés ou non, émanant des établissements d'enseignement et de recherche français ou étrangers, des laboratoires publics ou privés.



## 15 1. Introduction

16 Microplastics, commonly defined as plastics with the largest dimension below 5 mm (Collignon  
17 et al., 2014), are now readily recognized as ubiquitous in the environment. They can be directly  
18 produced for industrial use (i.e. primary source) or they can be generated by mechanical, pho-  
19 tochemical and/or biological degradation of larger plastic debris (i.e. secondary source). Most of  
20 the microplastics found in oceans derives from land-based larger plastic litter (Andrady, 2011). A  
21 series of recent reviews has described the growing threat of plastics pollution for marine ecosystems  
22 (Barboza and Gimenez, 2015; do Sul and Costa, 2014; Law, 2017; Rezania et al., 2018; Xanthos and  
23 Walker, 2017). Microplastics, by their similar dimension to sediments and planktonic organisms,  
24 can easily be mistaken for food and ingested by marine biota (Browne et al., 2008; Lima et al.,  
25 2014). Potential impacts of ingestion of microplastics are various, such as gut blockage, abrasion of  
26 the digestive system, reduced growth rates and reproductive deficiency (Galgani et al., 2010; Wright  
27 et al., 2013). In addition, microplastics can adsorb contaminants such as persistent organics and  
28 metals contained in the water (Bakir et al., 2014; Brennecke et al., 2016; Yonkos et al., 2014). Thus,  
29 organisms ingesting microplastics may assimilate sorbed contaminants, as well as toxic additives  
30 used in the compounding of plastics and bacteria encrusted on microplastics, leading to additional  
31 threats (Andrady, 2011). The ubiquity and abundance of microplastics increase the risks for ma-  
32 rine and estuarine ecosystems. Lima et al. (2014) showed that in the Goiana Estuary (Brasil) the  
33 quantity of microplastics in the water column can surpass the abundance of planktonic fish eggs  
34 and larvae.

35 Microplastics have been found in nearly every compartment of nearshore and open ocean sys-  
36 tems, including in the water column, sediments or living organisms (Crawford and Quinn, 2017;  
37 Cressey, 2016; Thompson et al., 2004; van Sebille et al., 2012). Nearly 96 % of the global amount  
38 of ocean microplastics originate in continents, i.e. mainly convected by rivers (Boucher and Friot,  
39 2017; Browne et al., 2011). Recently Lebreton et al. (2017) estimated that between 1.15 and 2.41  
40 million tons of plastic waste enter ocean every year through rivers. By their location at the in-  
41 terface between ocean and rivers, estuaries are of outstanding importance to gain knowledge on  
42 the dispersion mechanisms of microplastics. As estuaries are densely populated and industrialized,  
43 they represent an additional source of microplastics contamination. Understanding the behavior  
44 of plastics in estuarine environments is not simple and involves a range of processes which are not  
45 yet fully understood despite the growing number of dedicated studies. A common observation is  
46 that estuaries worldwide face microplastics contamination and have been identified as microplastics  
47 hotspots (Fok and Cheung, 2015; Simon-Sánchez et al., 2019). Experimental studies have been  
48 carried out in each aquatic compartment : biota (Abbasi et al., 2018; Browne et al., 2008; Li et al.,  
49 2018), water (Gallagher et al., 2016; Gray et al., 2018; Lima et al., 2015; Sadri and Thompson,  
50 2014; Xu et al., 2018; Yan et al., 2019; Yonkos et al., 2014; Zhao et al., 2015) and sediment (Gray  
51 et al., 2018; Naidoo et al., 2015; Peng et al., 2017; Simon-Sánchez et al., 2019; Willis et al., 2017).

52 For the water compartment, experimental and numerical approaches are generally limited to  
53 floating microplastics, such as surface sampling and 2D Lagrangian particle-tracking models coupled  
54 with ocean circulation models (Isobe et al., 2009; Kako et al., 2010; Lebreton et al., 2012; Murray  
55 et al., 2018; Neumann et al., 2014; Sherman and Van Sebille, 2016), assuming that most of the  
56 microplastics load is floating (Mani et al., 2015; McCormick et al., 2016; Yonkos et al., 2014), and  
57 focusing on the longitudinal spread of the plastics load from cities and sewage plants (Dris et al.,

58 2018; Mani et al., 2015). The floating-particle assumption is probably partly valid at large scale in  
59 the open ocean where most heavy particles would have sunk well beyond the resuspension (closure)  
60 depth. However, the vertical structure of the plastics load can certainly not be ignored in coastal  
61 and estuarine environments where the hydrodynamics is generally able to maintain in suspension  
62 sediments which are heavier than typical polymers (Forsberg et al., 2020; Jalón-Rojas et al., 2019;  
63 Kukulka et al., 2012). To numerically study the dispersion of microplastics in areas of intense  
64 turbulence or wave mixing, it was shown that vertical turbulence model and particle inertia are key  
65 parameters (Jalón-Rojas et al., 2019; Stocchino et al., 2019; DiBenedetto et al., 2018). The vertical  
66 structure of the microplastics load remains very poorly documented in the field, in particular in the  
67 presence of strong vertical variations of density and turbulent mixing such as observed in salt-wedge  
68 estuaries. While a growing research effort has been engaged to estimate the occurrence, distribution  
69 and composition of surface microplastics, no study has investigated the presence and abundance of  
70 microplastics along the vertical plane in estuarine systems. This issue is of particular importance in  
71 the challenging context of salt-wedge estuaries, where the competition between density stratification  
72 and turbulent mixing can drastically affect the behaviour of water masses and suspended particles.  
73 In the Adour Estuary, intense periods of mixing (i.e. ebb) followed by strong stratification periods  
74 (i.e. flood) have a great impact on the behaviour of suspended sediment (Defontaine et al., 2019).  
75 Similarly, microplastic distributions is expected to be strongly affected by the complex estuarine  
76 hydrodynamics, impacting the contamination of both inner estuary and connected coastal waters.

77 In addition, from a methodological point of view, the estuarine environment makes field sampling  
78 very difficult due to the variable bathymetry, intense currents and harbor activities. Commonly  
79 used sampling methods may be difficult to deploy in this environment. For instance small trawl  
80 nets (e.g. "Manta" nets), commonly used for surface water sampling, are generally towed at the  
81 rear of boats at a speed below 3 knots which is comparable or even lower than the surface ebbing  
82 velocities reached in a lot of estuaries. The repetition of trawling operations can also be greatly  
83 impaired by shipping and harbour operations. In such a complex context, numerical simulation can  
84 be a powerful tool to complete the understanding achieved through experimentation, to analyse the  
85 potential area of plastics accumulation and to help local authorities in taking appropriate actions  
86 to prevent and retrieve plastics pollution from the marine environment.

87 The Bay of Biscay is considered as an area of accumulation of marine litter due to specific  
88 circulation patterns (Declerck et al., 2019; Gago et al., 2015; Lebreton et al., 2012). However, data  
89 on microplastics distribution and abundance in this region are scarce, as shown by the review of  
90 Mendoza et al. (2020). Data collected during the PELACUS survey in the southern Bay of Biscay  
91 highlighted a medium level of contamination at the sea surface, in comparison with other areas  
92 of the world (Gago et al., 2015). The Adour River provides the main continental inputs for the  
93 coastal waters of the southeastern Bay of Biscay. Galgani et al. (2000) showed that the highest  
94 densities of litter on the sea floor in the Bay of Biscay were recorded in the area around the Adour  
95 Estuary. It was also suggested that the large amount of litter in Capbreton Canyon may be due  
96 to the proximity to the Adour Estuary. These observations raise the issue of the role played by  
97 the Adour Estuary in the contamination of coastal and regional waters by plastic litter, assumed  
98 to impact the rich local coastal ecosystems. The plastics load, including both micro-particles and  
99 larger litter, washed down by the Adour River into the Atlantic Ocean remains virtually unknown.

100 The main goal of the present paper is to analyze the microplastics distribution in a salt-wedge

101 estuarine system, including typical abundance, vertical structure and tidal dynamics. The focus is  
102 placed on a series of fundamental issues which have to date been rarely addressed: can microplas-  
103 tics be found everywhere in the water column, especially during periods of intense mixing? To  
104 what extent is traditional surface sampling able to provide a correct estimation of fluxes? Is the  
105 estuarine contamination associated with the river discharge and the flushing efficiency? Are the  
106 local hydrodynamics responsible for specific dispersion processes? For example, could the salt-  
107 wedge displacement affect the microplastics distribution and abundance, as it does with suspended  
108 sediments? In order to achieve a better understanding regarding these issues, the present study  
109 combines field sampling and numerical modelling at a selected field site of a major importance for  
110 the southeastern Bay of Biscay: the Adour estuary, France. The main novelties of the study are  
111 the dynamic characterization of the in-situ contamination throughout the water column and the  
112 use of an Eulerian approach to numerically simulate the dispersion processes for both neutrally and  
113 negatively buoyant microplastic particles, which have to date been rarely documented.

## 114 2. Methods

### 115 2.1. Field site

116 The Adour Estuary is a time dependent salt-wedge estuary (Defontaine et al., 2018, 2019; Sous  
117 et al., 2018) in the southern Bay of Biscay. The present study focuses on the lower 10 km of the  
118 estuary fed by the Adour River and the Nive River. The mouth is well sheltered by a 700 m long  
119 jetty at the entrance, strongly reducing the wave energy propagating into the estuary (Bellafont  
120 et al., 2018). Wind effect is expected to be mostly weak, due to overall low wind exposure with  
121 day-averaged values of less than 5  $m/s$  for 88 % of time (1980-2017 statistics from Meteo France).  
122 The S shape of the lower estuary further reduces the influence of the wind in the estuary. The  
123 mouth of the estuary is forced by a mesotidal regime, with a mean tidal range of 2.5 m. Tidal  
124 signal is semi-diurnal and its four major harmonic constituents are M2, S2, N2 and K2. The river  
125 discharge is quite variable, with an annual mean of about 300  $m^3/s$ , summer low discharge below  
126 80  $m^3/s$  and strong floods reaching more than 3 000  $m^3/s$  for the most extreme events. The  
127 estuarine dynamics are characterized by strongly variable density and velocity fields, impacting  
128 the transport of particles in suspension (Defontaine et al., 2019). The rising tide is associated  
129 with strong vertical density stratification, while the falling tide undergoes intense mixing periods  
130 responsible for a horizontal density gradient. The watershed is nearly 17,000  $km^2$  mostly composed  
131 of urban, agricultural and industrial areas, with a total population of one million inhabitants. The  
132 lower estuary studied here comprises the port of Bayonne and is flanked by the cities of Bayonne,  
133 Anglet and Boucau, being potential sources of microplastic contamination. More than 160 outflows  
134 are present in the port area both from civil (e.g. Waste Water Treatment Plants - WWTP, sewage  
135 network, rainwater network, storm water overflows) and industrial sources, some of which releasing  
136 untreated wastewaters. The location of the WWTP discharges are indicated in Figure 1 c).

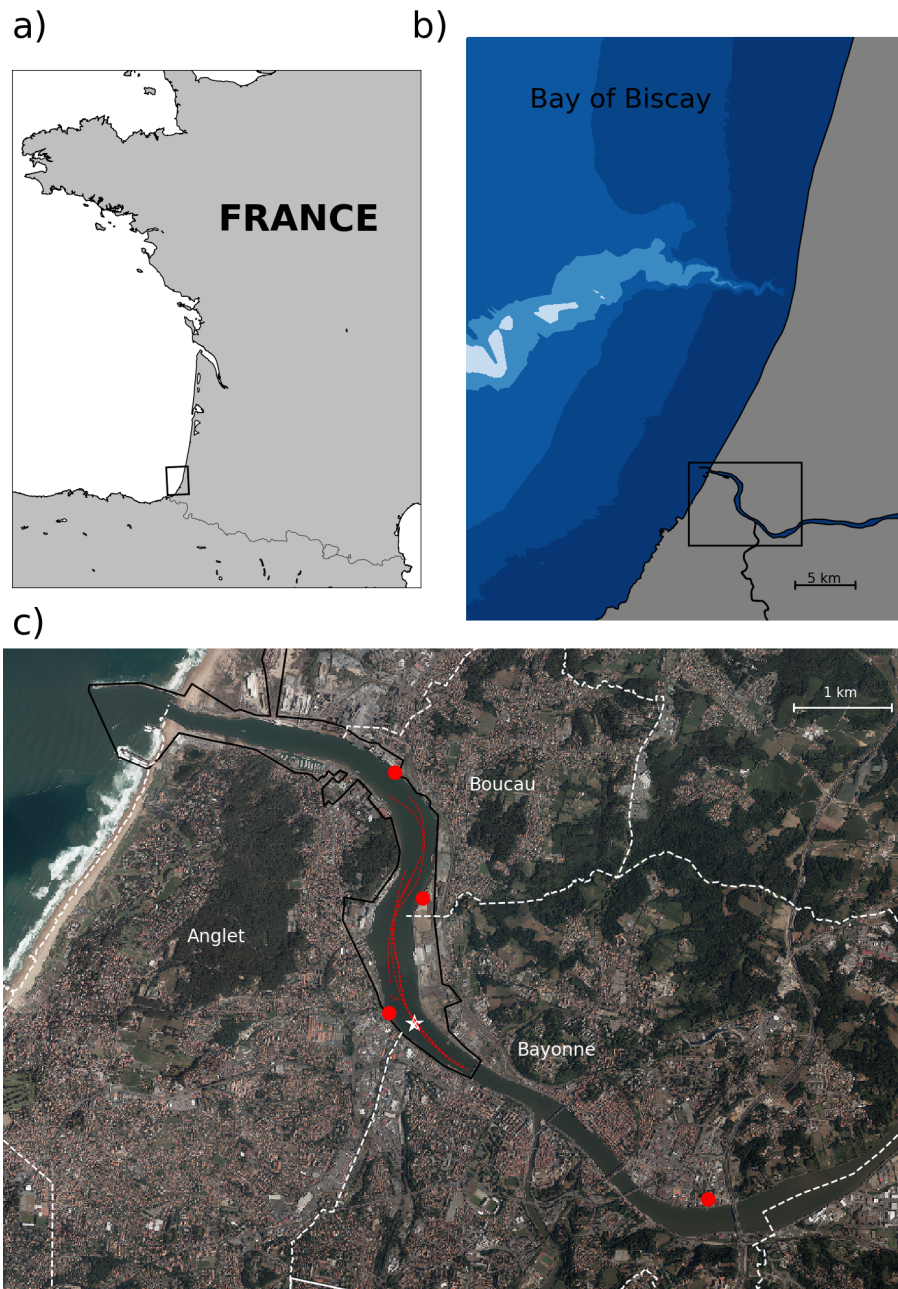


Figure 1: Location of the Adour estuary on the SW Coast of France (a) and more precisely on the Basque Coast (b). Sample location in Adour Estuary (c). The white star represents the anchored boat station. The red dashed lines represent the manta trawl. The thick black line represents the Bayonne port area. The red dots indicate the location of WWTPs outflows.

137 *2.2. Field sampling*

138 Sampling was undertaken from an anchored boat about 5 km from the mouth of the estuary  
 139 (Fig. 1 c)). This part of the estuary belongs to the port of Bayonne and is flanked by a densely  
 140 populated urban area. Sampling was conducted on June 6th, 2019 during a flood event and on  
 141 September 26th and 27th, 2019 during low river flow conditions. The river discharge rate was c.a.  
 142  $600 \text{ m}^3/\text{s}$  and  $85 \text{ m}^3/\text{s}$  during the June and September samplings, respectively. The river discharge

143 rate was estimated based on continuous river discharge survey performed by the French Water  
144 Agency ([www.hydro.eaufrance.fr](http://www.hydro.eaufrance.fr)) for the Adour River and its tributaries. The tidal range was 3.3  
145 m during June experiments and ranged from 2.6 m to 3.5 m during September experiments. The  
146 average wind magnitude and direction during the experiments were 4.1  $m/s$  at  $110^\circ$  on June 6, 3.4  
147  $m/s$  at  $330^\circ$  on September 26 and 1.7  $m/s$  at  $180^\circ$  on September 27. The water surface was flat,  
148 except for episodic events of boat wakes.

149 Methodological strategies to sample microplastics in the field are still open to debate. While  
150 there appears to be a consensus on the maximum size limit of 5 mm, the minimum size limit is  
151 highly dependent on the sampling and analysis methods employed. In surface waters, a manta trawl  
152 equipped with a standard  $300\mu m$  net is generally used (Gallagher et al., 2016; Sadri and Thompson,  
153 2014; Sutton et al., 2016; Yonkos et al., 2014; Zhao et al., 2014). Pumps may also be used to collect  
154 water samples that are then filtered in the laboratory with different sieve and filter sizes, enabling  
155 microplastics of smaller size to be taken into account (e.g. 45  $\mu m$  (Xu et al., 2018), 50  $\mu m$  (Yan  
156 et al., 2019), 63  $\mu m$  (Gray et al., 2018)). There is a wide range of methods for quantification and  
157 identification as shown in the reviews of Hidalgo-Ruz et al. (2012) and Cutroneo et al. (2020).  
158 There is still a need for standardization of definitions, sampling methods and analysis in order to  
159 achieve a common perspective and to dispose of comparable data sets at worldwide scale.

160 The sampling approach adopted here combined surface measurements, using a classical trawl  
161 net, with subsurface and near-bottom measurements using an immersed pump. For both measure-  
162 ment systems, the sampling duration and the related sampled volume were strongly constrained  
163 by two conflicting requirements. On one hand, large volumes would allow more statistically ro-  
164 bust results. On the other hand, the sampling duration is limited by the need to resolve in time  
165 the microplastics dispersion along the tidal cycle. The aim is to obtain successive samples over  
166 the tidal cycle representing a series of snapshots of the estuarine water contamination at different  
167 stages of the tidal cycles. The Adour Estuary is a tidally-driven intermittent salt-wedge estuary  
168 where strong variations in current properties (magnitude, direction, vertical shear, turbulent mix-  
169 ing) and density structure (potentially varying from fully filled by fresh or marine waters to a wide  
170 range of vertical density stratification patterns) can be observed. Each stage of the tidal cycle is  
171 therefore characterized by specific local hydrodynamic properties which are likely to affect the local  
172 microplastics contamination. The selection of the sampling duration was therefore intentionally  
173 limited to 30 min in order to capture the temporal estuarine patterns of change driven by tide  
174 and salt-wedge dynamics. The assumption is thus made that, for each sample, the hydrodynamic  
175 conditions can be considered as quasi-stationary. In addition, some of the sampling was interrupted  
176 before the targeted duration by port authorities for shipping purposes or by collisions with large  
177 sized floating litter. For the same reason, only the ebbing to low tide has been documented during  
178 the high discharge sampling (June) while a more complete description has been undertaken during  
179 the September experiment. These constraints finally result in sampling durations between 10 and  
180 30 min for both sampling methods described hereafter, namely the Manta net surface sampling and  
181 the subsurface and near bottom water pumping. Due to strong differences in sampling flux between  
182 surface net trawling and water pumping, this leads to wide differences in sampled volumes.

183 *2.2.1. Manta net sampling*

184 Surface water microplastics were collected with a manta trawl net with a rectangular opening 15  
185 cm high by 30 cm wide, and a 300  $\mu\text{m}$  mesh net. The net immersion was controlled by the lateral  
186 wings in such a way that 10 cm of the net mouth was underwater. Immersion depth fluctuations  
187 were visually estimated at about 2 cm. Typical sampling duration was 30 min with a tow speed of  
188 2 to 3 knots relatively to the water mass. The Manta net towing tracks followed approximately the  
189 main channel of the estuary, but differ in length due to the variability of surface current conditions.  
190 In a number of cases, the sampling was stopped either when the trawl mouth was obstructed by  
191 plant debris, branches or other macro-litter or when imposed by the port authorities. Samples with  
192 a duration of less than 10 min were discarded from the analysis. The manta trawl was equipped with  
193 a mechanical flowmeter to estimate the flow velocity, allowing calculation of standardized values  
194 per cubic meter. The sampled volumes varied from 45 to 146  $\text{m}^3$  with a relative uncertainty of  
195 about 20 % due to small fluctuations in the immersion depth. Surface conductivity and temperature  
196 were measured (van Essen CTD-diver<sup>®</sup> probe sampling at 1Hz) for each sample to estimate local  
197 salinity.

198 *2.2.2. Water pumping*

199 Subsurface and bottom water were sampled with a 750w immersed pump. Before each sampling,  
200 the pump discharge at the selected depth was first calibrated by timing the filling of a 0.5  $\text{m}^3$  tank.  
201 The pump, weighted by 20kg of lead, was positioned either in subsurface, i.e. approximately 1 m  
202 below the free surface, or in the near-bottom layer, i.e. approximately 1 m above the river bed. Due  
203 to the strong current, total control of the immersion depth was impossible but for each case the  
204 actual sampling depth was measured with an embedded pressure sensor (van Essen CTD-diver<sup>®</sup>  
205 sampling at 1 Hz). Conductivity and temperature were also measured with the same probe for each  
206 sample to estimate local salinity at the depth reached. The pumped water was poured through two  
207 successive sieves of 5 mm and 300  $\mu\text{m}$  in order to provide pre-sorted samples. The pumped volume  
208 varied from 2.8 to 5.1  $\text{m}^3$ .

209 *2.3. Analysis*

210 After sampling, additional separation is required to identify and quantify microplastics from the  
211 water samples. Recent reviews show that the most common techniques are visual sorting, density  
212 separation and filtration which can be combined to varying degrees or completed by finer anal-  
213 ysis such as Fourier-Transform Infrared Spectroscopy (Alvim et al., 2020; Cutroneo et al., 2020).  
214 The identification is performed here by visual inspection and separation using a binocular magnifier  
215 (Leika M165C) and metal tweezers. Used alone, this approach would be inappropriate for microplas-  
216 tics below 100  $\mu\text{m}$  (Lenz et al., 2015). For the size range studied here ( $>300 \mu\text{m}$ ), polymer particles  
217 are generally straightforward to discriminate from mineral or vegetal particles by an experienced  
218 operator on the basis of brightness, hardness, stiffness and absence of striation (Covernton et al.,  
219 2019). Recent intercomparisons provided an estimation of the related identification uncertainty, of  
220 about 14 % (Cadiou et al., 2020). Each sample was sorted on a petri dish, the microplastics isolated  
221 and finally dried in an oven at 45<sup>o</sup>C during 24h. Microplastic characterization was performed by  
222 imaging. Dried fragments were digitally recorded with a Zooscan device. After this, counts and  
223 maximum length were determined through Image J and Plankton identifier. Microplastics were  
224 classified into five categories of shape, namely spheres, fibers, fragments, films and others.

## 225 2.4. Numerical model

### 226 2.4.1. Hydrodynamics

227 The simulations were run with a TELEMAC-3D numerical model from the open source TELEMAC-  
228 MASCARET<sup>®</sup> modelling system. TELEMAC-3D solves the free surface Navier-Stokes equation  
229 (Hervouet, 2007). The hydrostatic pressure hypothesis and the Boussinesq approximation on the  
230 density were taken into consideration in the momentum equation. The turbulent closure model is  
231 based on a turbulent viscosity concept using the Prandtl formulation of the mixing length theory.  
232 The Munk Anderson damping function, decreasing with the value of the Richardson number, was  
233 used to reproduce the damping of turbulent mixing due to density stratification. An unstructured  
234 triangular mesh was created on Blue Kenue<sup>®</sup> covering the Basque country coast and the Adour  
235 and Nive Rivers, with cells from 30 m to 2000 m (Fig. 2). The finest resolution (30 m cells) was  
236 inside the lower Adour Estuary (i.e. corresponding to the field experimentation site). The grid  
237 covered the ocean up to 40 km from the estuary mouth and it extended up to 70 km in the Adour  
238 and 25 km in the Nive River. The vertical dimension was resolved with 20 equidistant sigma coor-  
239 dinate layers. At the marine boundary, tidal forcing was imposed at each node using 11 harmonic  
240 constituents of the TPXO data base. The tidal range imposed during the simulations was 3.5 m,  
241 i.e. close to the field conditions. At both riverine boundaries, a river discharge was forced. Two  
242 river flow conditions were considered to mimic the field conditions : low river flow corresponding  
243 to the September sampling, with the Adour and Nive Rivers flow of 90 and 10  $m^3/s$ , respectively,  
244 and high river flow corresponding to the June experiment, with the Adour and Nive Rivers flow of  
245 525 and 75  $m^3/s$ , respectively. No wind or wave forcing was considered in the present simulations.  
246 The initial conditions consist in the last time step of a previous computation of 25 days sufficient  
247 to establish the flow and the salinity structure (Defontaine, 2019). The model was calibrated and  
248 validated based on tidal gauge data (five gauges), two bottom-moored ADCP data and density  
249 profiles collected in 2017 and 2018; for further details refer to Defontaine (2019).

### 250 2.4.2. Microplastics dispersion

251 Microplastics were treated as passive tracers with concentrations that changed with time and  
252 space by solving the advection-diffusion equation with an additional settling velocity. The turbulent  
253 diffusion coefficient of microplastics is assumed to be the same as for turbulent momentum diffusion,  
254 i.e. corresponding to a turbulent Schmidt number of 1. Three types of particles were considered for  
255 simulations to explore the effect of mean diameter, density and settling velocity on the dispersion.  
256 The parameters used in S1 and S2 simulations (see Table 1) are typical values recovered from  
257 laboratory measurements presented in the literature : S1 is representative of a polystyrene sphere of  
258 0.5 mm (density = 1.05  $g/cm^3$ ) (Kowalski et al., 2016) and S2 is representative of a polycaprolactone  
259 sphere of 4.9 mm (density = 1.13  $g/cm^3$ ) (Khatmullina and Isachenko, 2017). For simulation S3,  
260 an idealized neutrally-buoyant particle of 3 mm is considered with a density equal to fresh water  
261 density.

### 262 2.4.3. Simulation runs

263 Each model run was 9 days long. In order to understand the dispersion of microplastics in a  
264 time-dependent density-stratified water mass, a single patch of microplastics was released at a given  
265 point of the lower estuary on day 4 at high tide during 15 minutes, with a concentration of 10  $g/L$ .

266 The source was located on the right bank at the level of Bayonne city (Fig. 2), at zero meters above  
 267 the chart datum. Each type of simulation was run twice, in high and low river flow conditions,  
 268 amounting to 6 simulations. Four Eulerian control points were used to monitor the changes over  
 269 time in concentrations, see Figure 2. C1 was located at the river mouth to analyse exchanges with  
 270 the ocean, C2 was in front of the initial release point and C3 and C4 were upstream in the Nive  
 271 River and Adour River, respectively, to monitor the time-varying microplastics distribution.

Table 1: Microplastic characteristics used for simulations.

<i>Simulation name</i>	<i>Mean diameter (mm)</i>	<i>Density (g/cm<sup>3</sup>)</i>	<i>Settling velocity (mm/s)</i>
S1	0.5	1.05	4
S2	4.9	1.13	127
S3	3	1.00	0

#### 272 2.4.4. Numerical products

273 In addition to the direct analysis of concentrations, the numerical results were processed using  
 274 two non-dimensional numbers, namely the Richardson number and the Rouse number.

275 The Richardson number  $Ri$  estimates the relative importance of the gravitational effects induced  
 276 by the density gradient and the vertical shear on the stability of the water column. It is expressed  
 277 as :

$$278 \quad Ri = -\frac{N^2}{S^2} \quad (1)$$

279 where  $N^2 = -\frac{g}{\rho_0} \partial \rho / \partial z$  is the Brunt-Väisälä frequency,  $g$  is the gravity acceleration,  $\rho_0$  is the  
 280 reference density and  $S = \partial \bar{u} / \partial z$  is the vertical shear of the mean horizontal velocity. The buoyancy  
 281 forces induced by the vertical density gradient are assumed to overcome turbulent mixing due to  
 282 shear stress when the Richardson number is above the threshold value of 0.25. By contrast, an  
 283 unstable configuration induced by the stratification breakdown by the turbulent mixing is expected  
 284 for values of the Richardson number below 0.25.

285 The Rouse number  $Ro$  is defined as the ratio of the settling velocity to the shear flow:

$$286 \quad Ro = \frac{w_s}{\kappa u^*} \quad (2)$$

287 where  $w_s$  is the settling velocity,  $\kappa$  is the Von Karman's constant and  $u^*$  is the shear velocity. It  
 288 is generally used to determine the mode of sediment transport with several thresholds: bed load  
 289 ( $Ro > 2.5$ ), 50% suspended ( $1.2 < Ro < 2.5$ ), 100% suspended ( $0.8 < Ro < 1.2$ ) and wash load  
 290 ( $Ro < 0.8$ ).

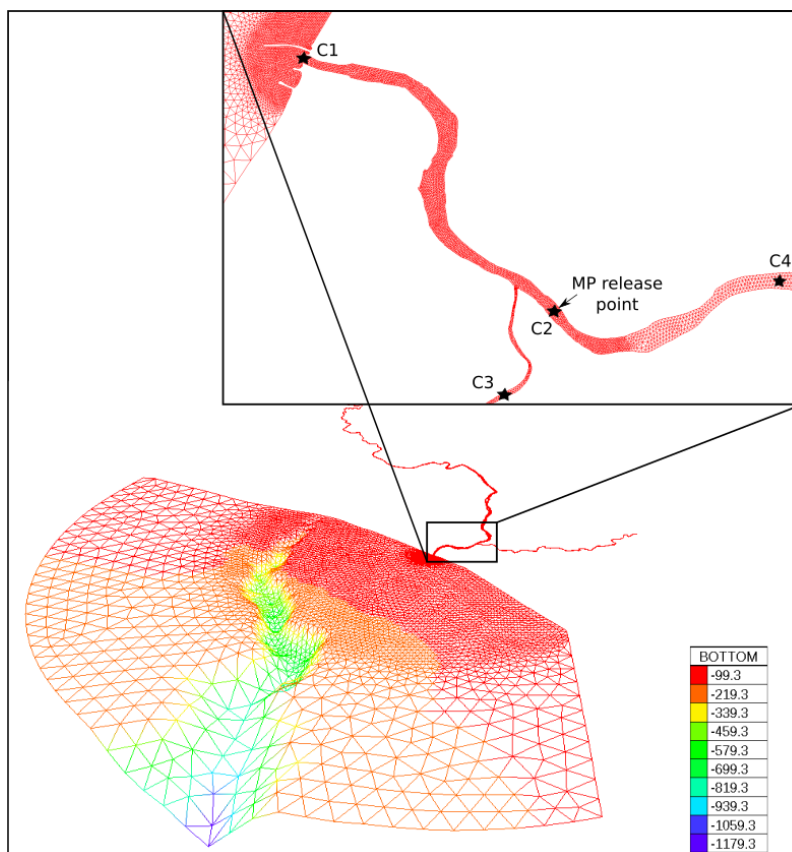


Figure 2: 3D view of the mesh grid, with a top-view zoom on the lower part of the estuary where the measurements took place, colours corresponding to the bed level in meters. The black arrow shows the location of numerical microplastics release. C1 to C4 are control points where simulated concentrations of microplastics are retrieved for data analysis.

### 291 3. Results

#### 292 3.1. Field observations

293 A total of 669 microplastic particles were collected during this study. Only one sample out of a  
 294 total of fifteen (6.7%) was free of microplastics. The average number of microplastics per sample  
 295 was 126 for trawl and 4 for pumped sampling, respectively, reflecting the difference in sampled  
 296 volumes. Concentration of microplastics found in the samples ranged from 0 to  $3.88 \text{ part}/\text{m}^3$ , with  
 297 a mean and median abundance of  $1.13$  and  $0.81 \text{ part}/\text{m}^3$  (standard deviation  $1.12 \text{ part}/\text{m}^3$ ).

298 A first striking observation is that microplastics were present throughout the water column  
 299 with similar levels of contamination. Mean abundance for surface and subsurface layers over both  
 300 discharge conditions were  $1.18$  and  $0.89 \text{ part}/\text{m}^3$ , respectively. Corresponding median values and  
 301 standard deviations are  $0.94$  and  $0.98 \text{ part}/\text{m}^3$  for the surface layer and  $0.2$  and  $1.67 \text{ part}/\text{m}^3$  for  
 302 the subsurface layer. The highest mean abundance of  $1.26 \text{ part}/\text{m}^3$  was found near the bottom  
 303 waters, with a median value of  $1.23 \text{ part}/\text{m}^3$  and a standard deviation of  $1.04 \text{ part}/\text{m}^3$ .

304 High river flow was associated with higher depth-averaged concentration (mean of  $1.60$ , median  
 305 of  $1.41$  and standard deviation of  $1.28 \text{ part}/\text{m}^3$ ) than low discharge conditions (mean of  $0.96$ ,  
 306 median of  $0.58$  and standard deviation of  $1.06 \text{ part}/\text{m}^3$ ). This is probably due to a combination of

307 several factors, including higher land and city drainage during flood and/or sewage treatment plants  
 308 discharge. It should be stressed that even if the overall order of magnitude for the concentration  
 309 remained within the same range, the difference in river discharge between the June and September  
 310 experiments led to a much stronger net export flux for the high discharge conditions.

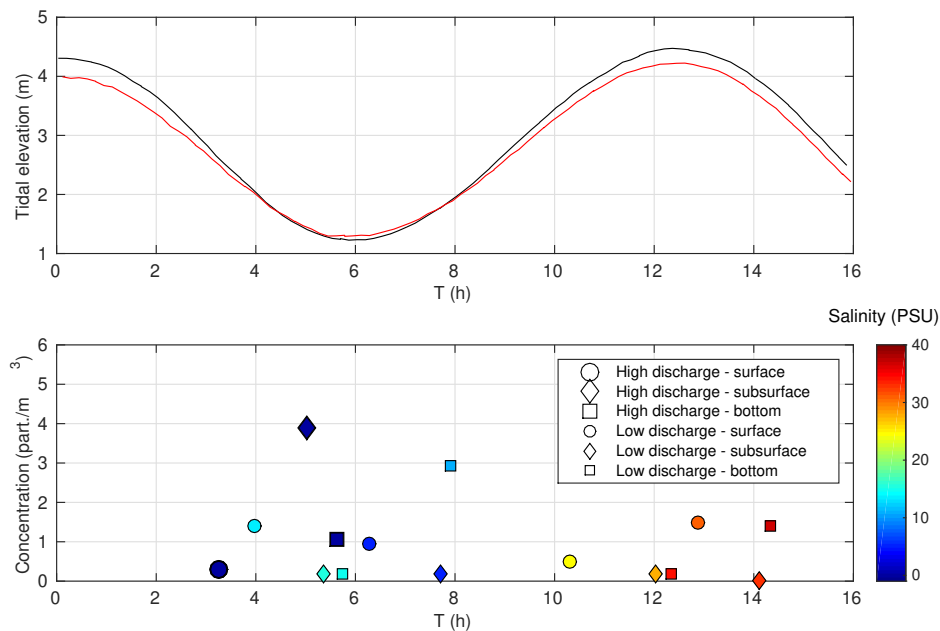


Figure 3: Tidal evolution of microplastics concentrations for low and high discharge events. Top: tidal elevation for low (September, in red) and high (June, in black) discharge conditions. Bottom: measured concentrations for low (small symbols) and high (large symbols) discharge conditions. Surface, subsurface and bottom measurements are denoted by circles, diamonds and squares, respectively. The ambient salinity (PSU) at the sampling depth is shown by the colour level.

311 The tidal evolution of microplastics concentrations through the water column are presented  
 312 in Figure 3. Salinity values showed that, during low discharge conditions, the estuary was filled  
 313 with riverine fresh/marine salty waters around low/high tide, respectively. A small vertical density  
 314 stratification was present at rising tide for low discharge condition, see the salinity gradient just  
 315 before 8 h between subsurface (diamond,  $S=4.9$ ) and bottom (square,  $S=10.8$ ) measurements. For  
 316 high discharge conditions (large symbols), marine waters were totally expelled from the estuary  
 317 during the ebb tide. For more detailed information on the estuarine hydrodynamics, the reader  
 318 can refer to Defontaine et al. (2019). Figure 3 first reveals that, in most cases, the microplastics  
 319 concentration fluctuated between 0.2 and  $2 \text{ part}/\text{m}^3$  regardless of the discharge and tidal conditions,  
 320 the ambient salinity and of the position in the water column. This consolidates the mean order  
 321 of magnitude previously mentioned. The identification of finer trends, either over time or through  
 322 the water column was not straightforward. Two peaks of concentration were however observed  
 323 outside this typical range. The first was for high discharge conditions at the end of the ebb, where  
 324 subsurface concentrations were observed at  $3.9 \text{ part}/\text{m}^3$  and the second at  $2.9 \text{ part}/\text{m}^3$  was observed  
 325 in the near bottom layer at the beginning of the rising tide in low discharge condition. While these  
 326 peaks could have been caused by a number of factors including variation in external inputs, the

327 local hydrodynamics could play a significant role in the peak development. Defontaine et al. (2019)  
 328 have shown that late ebb corresponds to a peak of velocity and turbulent mixing responsible for  
 329 massive sediment resuspension events reaching the surface. This could affect the concentration of  
 330 microplastics in a similar manner, as observed by the former peak of microplastics concentrations  
 331 ( $3.9 \text{ part/m}^3$ ). The latter peak ( $2.9 \text{ part/m}^3$ ) could be attributed to the deposition mechanism  
 332 observed at the beginning of the rising tide when a minimum of velocity is reached (i.e. current  
 333 reversal) (Defontaine et al., 2019).

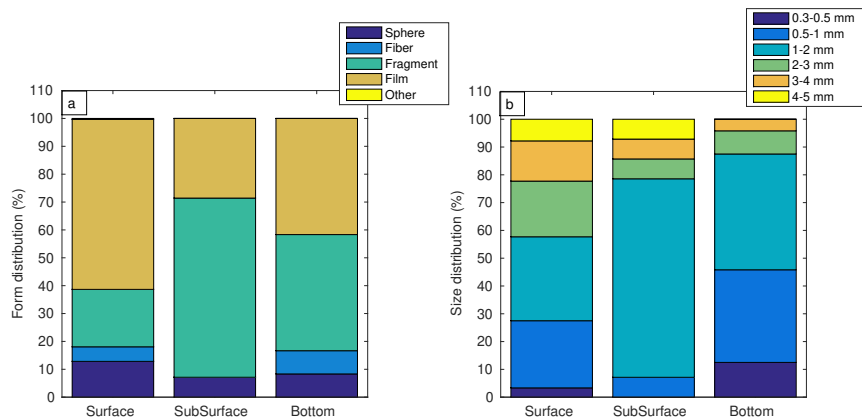


Figure 4: Distribution of forms (a) and sizes (b) of the sampled microplastic particles in surface, subsurface and bottom layers.

334 Figure 4 depicts the shape (a) and size (b) distributions of the sampled microplastics. Films  
 335 and fragments were the predominant types of microplastics found in the lower Adour Estuary,  
 336 respectively 59.6% and 22.3%, followed by spheres found at 12.6 %. The form distribution in the  
 337 surface was similar to the depth-averaged one, reflecting the difference in sampled volumes. In  
 338 subsurface layer, fragments were clearly predominant while fibers were absent. In the bottom layer,  
 339 fragments showed similar levels to films, with a small proportion of fibers and spheres.

340 The size distribution (Fig. 4 right panel) was also depth-variable. Surface distribution was the  
 341 most balanced with the 0.5-1, 1-2 and 2-3 mm classes sharing about 75 % of the particles. The  
 342 subsurface layer was characterized by the absence of very fine (0.3-0.5mm) particles and the clear  
 343 dominance of the 1-2 mm class while an overall shift toward finer particles was observed near the  
 344 bottom.

### 345 3.2. Numerical results

346 A series of numerical simulations have been performed to provide further insight on the spatial  
 347 and temporal dynamics of microplastics with variable properties, see table 1. The objective was  
 348 to track the dispersion of a single patch of microplastics released at a source point during a short  
 349 time period. The following analysis was based on a longitudinal section of concentrations, salinity,  
 350 Richardson number and Rouse number at mid falling and rising tides for the three types of particle  
 351 for low and high river discharge conditions (Figures 5 and 6, respectively), tidal evolution of water  
 352 column stability (Richardson number) and transport capacity (Rouse number) for the S1 case

353 (Figure 7) and time evolution of concentrations at four selected control points in the estuarine  
354 system during low and high river discharge conditions (Figures 8 and 9, respectively).

355 Microplastics, like any particle in suspension, are very sensitive to hydrodynamics. Therefore,  
356 tidal currents are of the utmost importance for the transport of microplastics in suspension. Mi-  
357 croplastics were transported in an oscillating manner, upstream and downstream in the estuary  
358 following the tidal motion (Figs. 8 and 9). The patch of microplastics moved downstream during  
359 the falling tide and upstream during the rising tide. One part of the microplastics patch moved  
360 into the Nive River during the rising tide. Thus, the Nive River could become contaminated by  
361 microplastics released into the Adour River. Different peaks of concentration can be observed in  
362 Figures 8 and 9.

363 Defontaine (2019) showed that peaks of sediment concentrations are correlated with periods of  
364 maximum velocity and peaks of turbulent mixing. A similar pattern of behaviour for microplastics  
365 is confirmed by the present numerical results. Focusing on S1 simulation with microplastics heavier  
366 than marine water and having a low settling velocity (Figs. 5 g) and h) and Figs. 6 g) and  
367 h), the salinity field strongly affects the resuspension mechanism. During the rising tide, the  
368 strong density stratification typical of the salt-wedge structure damps the turbulent mixing and  
369 thus contains the transport in suspension below the pycnocline (Figs. 5 h) and 6 h)). During  
370 the falling tide, the typical periods of intense mixing led to greater vertical spreading and more  
371 homogeneous concentration through the vertical (Figs. 5 g) and 6 g). These alternating periods of  
372 resuspension/deposition over the tidal cycle are clearly visible in Figure 7. At the end of the ebb tide,  
373 the water column is unstable ( $Ri < 0.25$ , i.e. periods of intense mixing), favoring the transport of  
374 microplastics in suspension ( $Ro < 2.5$ ) throughout the whole water column (i.e. high concentration  
375 of microplastics at the surface). At the beginning of the rising tide, the water column is well-mixed  
376 ( $Ri < 0.25$ ), but the current reversal is associated with a strong reduction of the transport capacity  
377 ( $Ro > 2.5$ ) inducing microplastics deposition on the bed. At mid flood tide, the salt-wedge entrance  
378 results in a highly stratified and stable water column. The resuspension is thus contained by the  
379 pycnocline with a drop in mid and surface concentrations. At the end of the flood tide, the peak  
380 of the Rouse number indicates the reversal of the current and its associated deposition process.

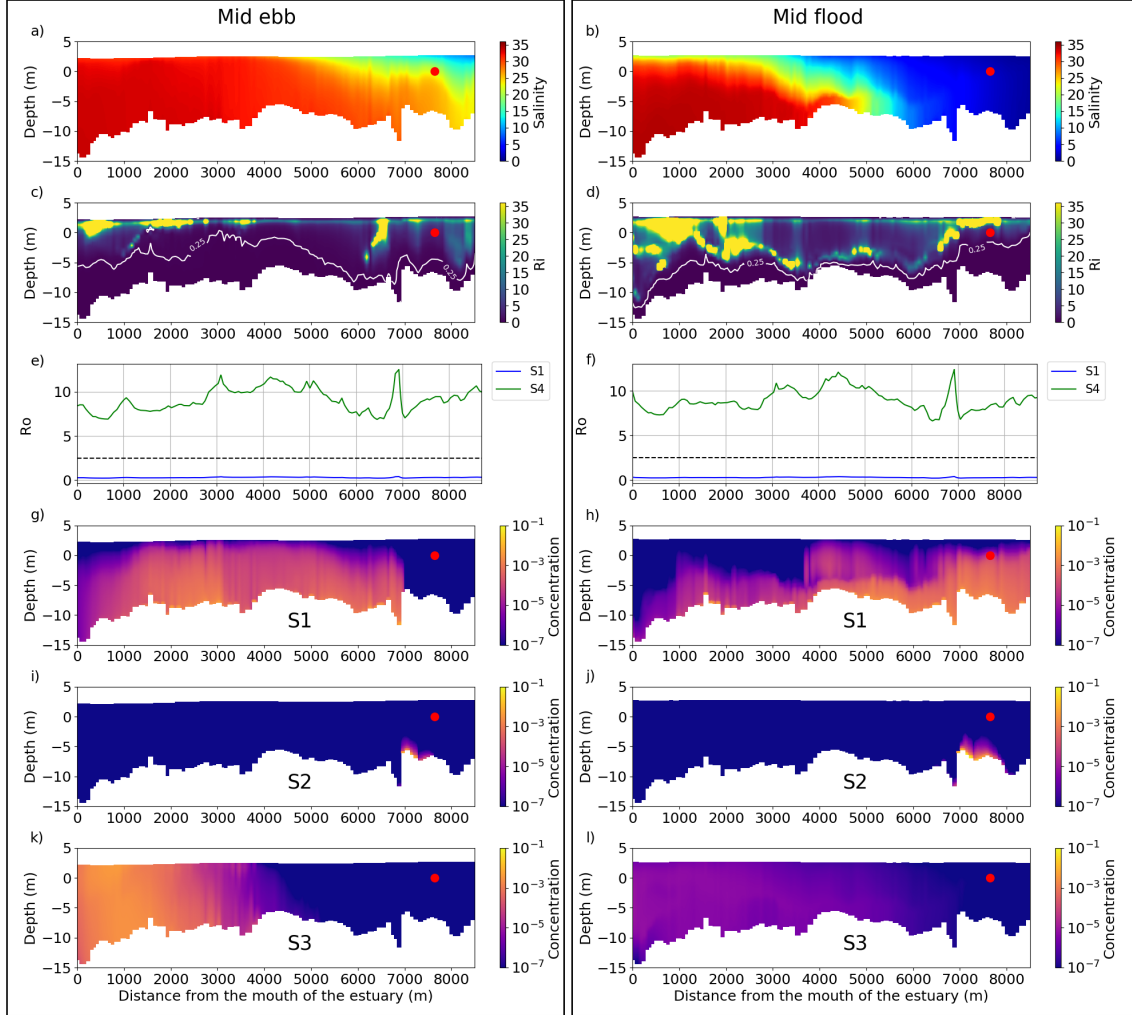


Figure 5: a) and b) : longitudinal section of salinity at mid falling and rising tides. c) and d) : longitudinal section of the Richardson number, the white line indicates the threshold value of  $Ri = 0.25$  between stable and unstable configurations. e) and f) : time series of Rouse number for the simulation S1 (blue) and S2 (green), the dashed line indicates the threshold value of  $Ro = 2.5$  between bed load transport and transport in suspension. g) to l) : longitudinal section of microplastics concentrations in g/L for the three simulation runs (S1,S2 and S3). Data were extracted about three hours (mid ebb = left panel) and nine hours (mid flood = right panel) after the microplastic release on Day 4 under low river discharge conditions. On longitudinal sections the red dot indicates the location of the microplastics release.

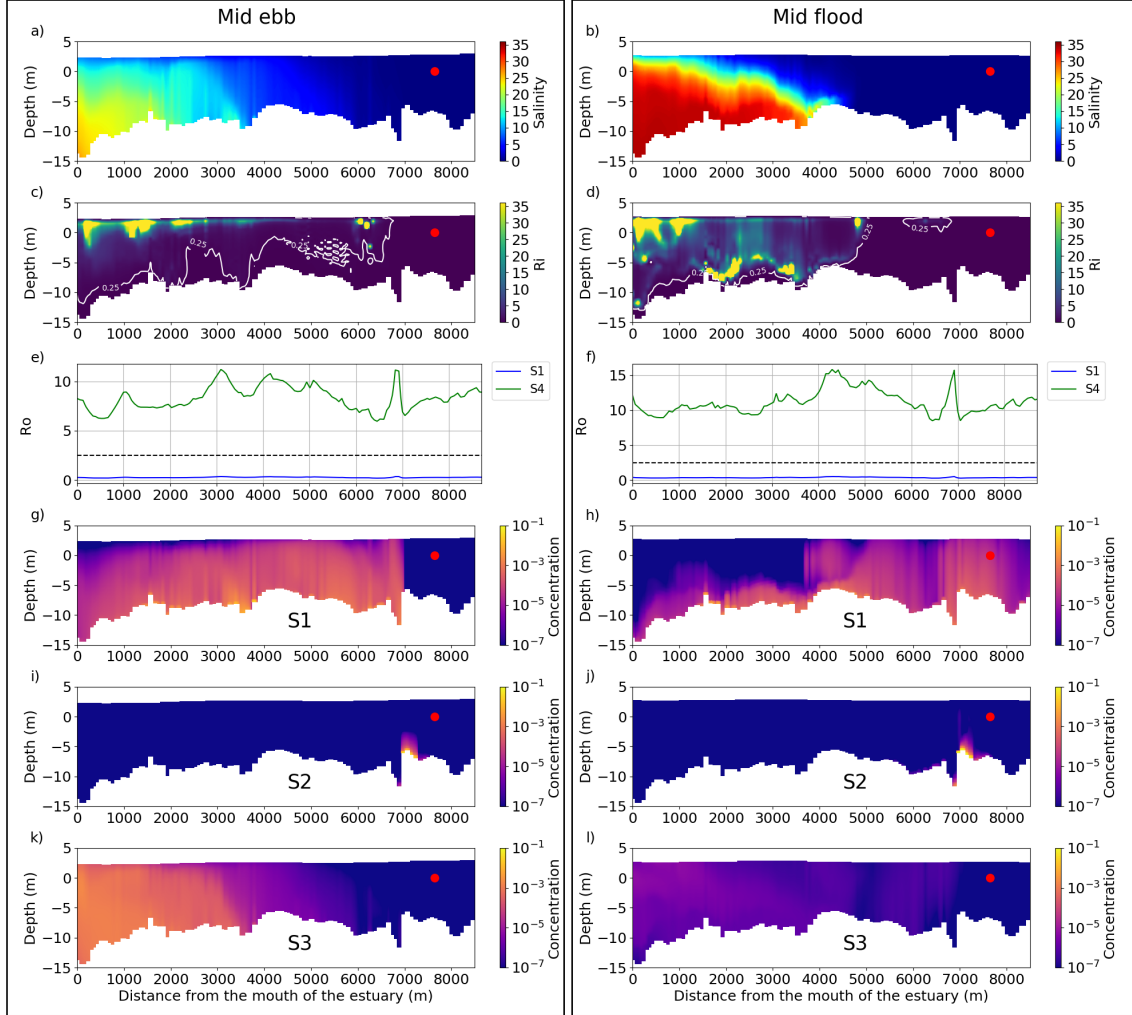


Figure 6: a) and b) : longitudinal section of salinity at mid falling and rising tides. c) and d) : longitudinal section of the Richardson number, the white line indicates the threshold value of  $Ri = 0.25$  between stable and unstable configurations. e) and f) : time series of Rouse number for the simulation S1 (blue) and S2 (green), the dashed line indicates the threshold value of  $Ro = 2.5$  between bed load transport and transport in suspension. g) to l) : longitudinal section of microplastics concentrations in g/L for the three simulation runs (S1,S2 and S3). Data were extracted about three hours (mid ebb = left panel) and nine hours (mid flood = right panel) after the microplastic release on Day 4 under high river discharge conditions. On longitudinal sections the red dot indicates the location of the microplastic release.

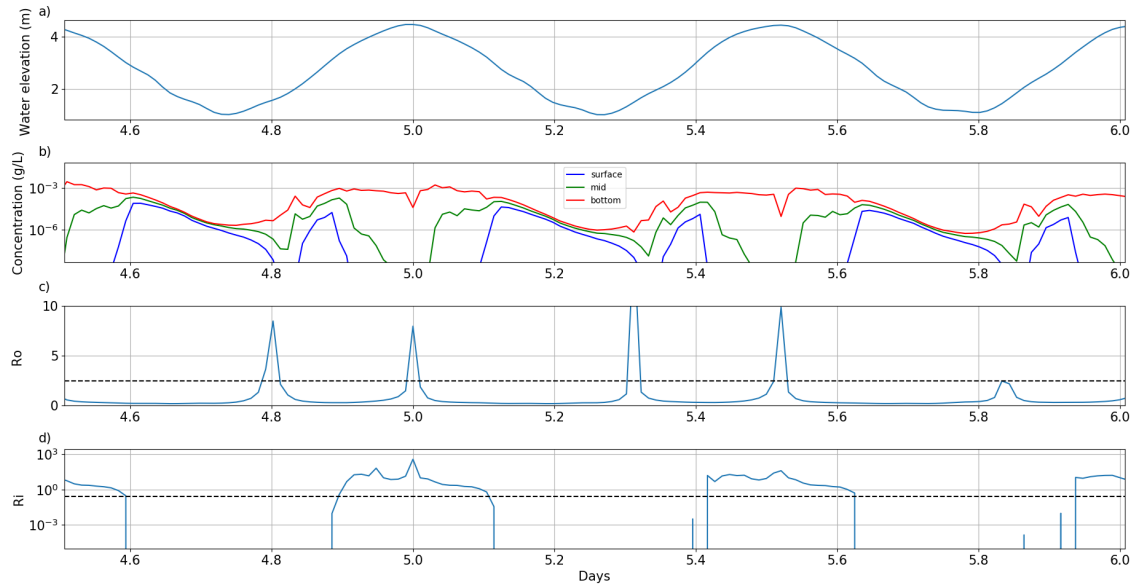


Figure 7: Time series of a) water elevation (m), b) microplastics concentrations (g/L), c) Rouse number and d) vertically averaged Richardson number. The dashed lines indicate the threshold values for the Rouse number  $Ro = 2.5$  and the Richardson number  $Ri = 0.25$ . Data were extracted from S1 simulation in high river flow conditions at the C2 control point.

381 Microplastics transport was also affected by their inner characteristics : size, density and as-  
 382 sociated settling velocity. Neutrally-buoyant microplastics easily spread through the entire water  
 383 column and they were more affected by tidal flushing (Figs. 8 c and 9 c). They were flushed from  
 384 the estuary within few tidal cycles, while heavier microplastics tend to stay in the estuary. The  
 385 good flushing capacity of neutrally-buoyant microplastics can be explained by the actions, during  
 386 the rising tide, of a two-layer flow with marine waters entering into the estuary bottom layers and  
 387 riverine waters flowing out of the estuary at the surface and, during the falling tide, an outflow of  
 388 the full water column. The surface waters are thus almost permanently flowing out the estuary.  
 389 Neutrally-buoyant microplastics being generally more concentrated in the surface layer than heav-  
 390 ier microplastics, their residence time is reduced. Microplastics with a density higher than that of  
 391 marine water but a low settling velocity (S1) spread along the Adour and Nive Rivers (i.e. from  
 392 C1 to C4), with a gradient of concentration from surface to bottom (Fig. 8 and 9 a, d, g and  
 393 j). Microplastics leaving the estuary during the ebb were re-injected by coastal waters during the  
 394 following flood tide. This re-injection of microplastics during the rising tide is partly due to the  
 395 fact that longshore currents, wave and wind forcing in the coastal area were not considered in the  
 396 simulations. Dense microplastics with a high settling velocity (S2) sank at the level of the source  
 397 point. They just moved back and forth over a short distance close to the source point. They were  
 398 re-suspended and deposited by the salt-wedge displacement, but they were never flushed out of the  
 399 estuary.

400 The difference between low and high river flow conditions is straightforward in figures 8 and 9.  
 401 Microplastics flushing was faster with high river flow and the upward displacement of microplastics  
 402 was reduced. In simulations S2 and S3, microplastics were not able to reach the C4 control point  
 403 during the rising tide under high river flow (Fig. 9). In simulation S1, the concentrations at C2, C3

404 and C4 clearly decreased with time during high river flow conditions. The higher concentrations of  
 405 microplastics were localised at the entrance of the estuary (i.e. C1 and C2), while during the low  
 406 river discharge the higher concentrations were upward at C3 and C4. This pattern was similar to  
 407 that of an estuarine turbidity maximum (ETM), which generally moves downstream during high  
 408 river flow and upward during low river flow (Burchard et al., 2018).

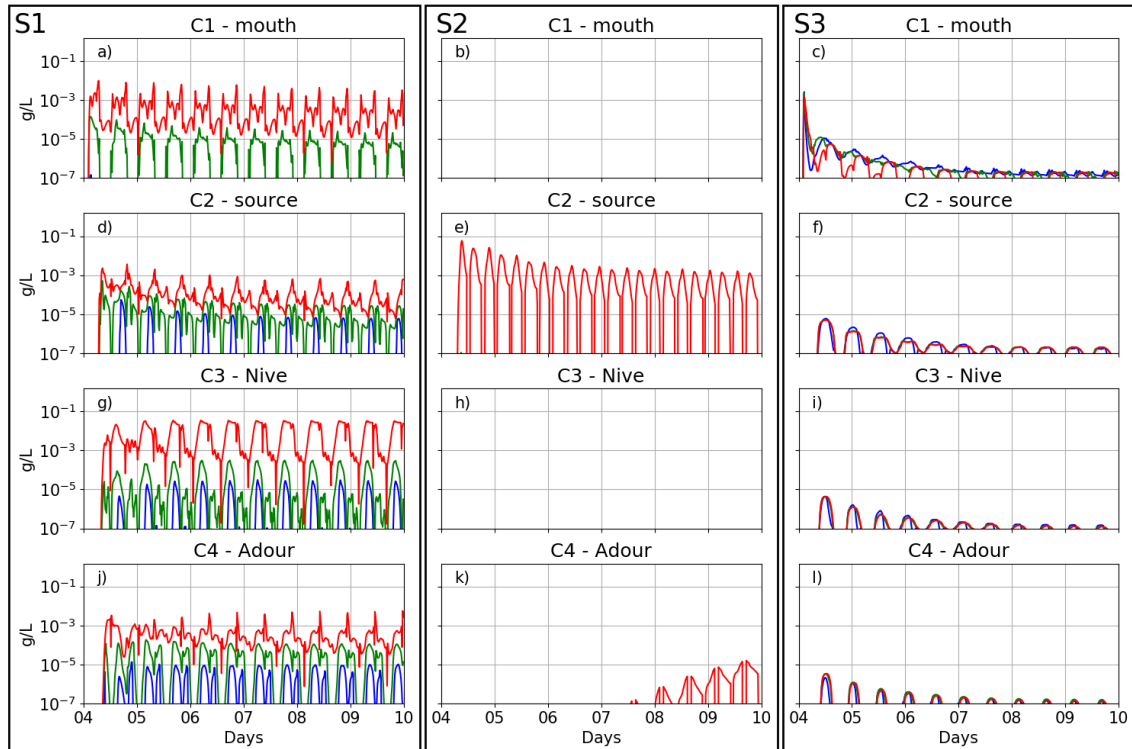


Figure 8: Concentrations in microplastics during low river discharge condition. The four rows correspond to the four control points: C1 (mouth of the estuary), C2 (close to numerical release point), C3 (upstream Nive River) and C4 (upstream Adour River). The three columns correspond to the three types of simulated particles: S1 for (a), (d), (g), (j), S2 for (b), (e), (h), (k) and S3 (c), (f), (i) and (l)). Red, green and blue lines correspond to bottom, mid-column and surface concentrations (g/L), respectively.

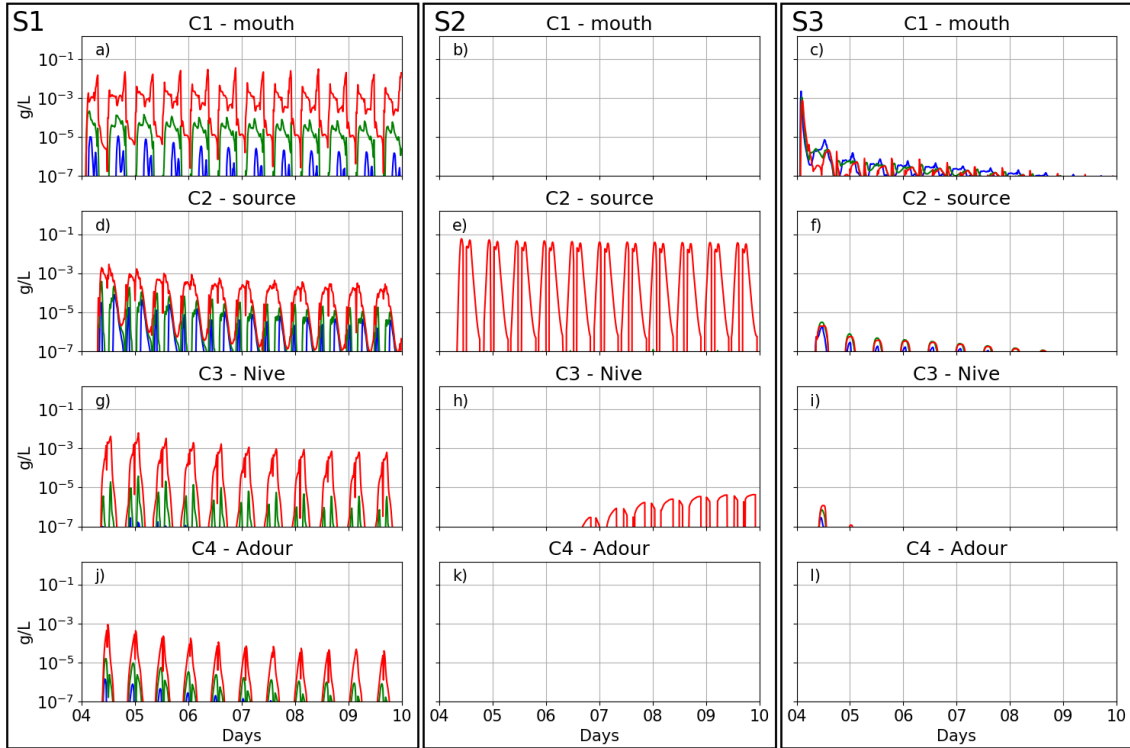


Figure 9: Concentrations in microplastics during high river discharge condition. The four rows correspond to the four control points: C1 (estuary mouth), C2 (release point), C3 (upstream Nive River) and C4 (upstream Adour River). The three columns correspond to the three types of simulated particles: S1 for (a), d), g), j), S2 for (b), e), h), k) and S3 (c), f), i) and l)). Red, green and blue lines correspond to bottom, mid-column and surface concentrations (g/L), respectively.

#### 409 4. Discussion

410 Discussion points are organized in four main topics: microplastics abundance and fluxes, in-  
 411 fluence of microplastics properties on their dispersion, influence of the salt-wedge dynamics on  
 412 microplastics dispersion and simulation hypothesis and limitations.

##### 413 4.1. Microplastics abundance and fluxes

414 The present field sampling provided the first estimation of microplastics abundance in the Adour  
 415 Estuary with a mean value of  $1.13 \text{ part}/m^3$ . For the sake of comparison, microplastics contamina-  
 416 tion levels reported in other estuaries are summarized in Table 2. European estuaries have lower  
 417 to comparable levels of contamination, while field studies in Asia and USA reported higher values  
 418 of contamination, up to four orders of magnitude higher. Note also that the microplastics abun-  
 419 dance in the Adour estuary is similar to the subsurface water abundance in the Bay of Biscay.  
 420 Nevertheless, inter-site comparisons should be undertaken with caution due to the lack of standard-  
 421 ization regarding the definition of microplastics, particularly regarding the size and the sampling  
 422 techniques. Apart from the methodological issue of collection techniques discussed previously, the  
 423 difference in contamination levels between estuaries is likely due to anthropogenic pressure which  
 424 can be approximated with the size and the use of the watershed and the size of adjacent urban

425 areas. Microplastics pollution is significantly correlated with the proximity to and the size of urban  
 426 areas (Gago et al., 2015; Lebreton et al., 2017; Naidoo et al., 2015; Rodrigues et al., 2019; Yonkos  
 427 et al., 2014).

Table 2: Reported microplastics abundance for estuaries around the world and the Bay of Biscay.

<i>Location</i>	<i>Mean concentration (part/m<sup>3</sup>)</i>	<i>Depth</i>	<i>Sampling method</i>	<i>Size</i>	<i>Reference</i>
Tamar Estuary (UK)	0.028	Surface	Manta net	[300 $\mu$ m - 5 mm]	Sadri and Thompson (2014)
Douro Estuary (Portugal)	0.17	Subsurface (1-2 m)	Conical	[30 $\mu$ m - 500 $\mu$ m]	Rodrigues et al. (2019)
Ebro Estuary (Spain)	3.5	Surface	Neuston net	[5 $\mu$ m - 5 mm]	Simon-Sánchez et al. (2019)
Changjiang Estuary (China)	231	Subsurface (50cm)	Pumping	[70 $\mu$ m - 5 mm]	Xu et al. (2018)
Minjiang Estuary (China)	1246	Subsurface (30 cm)	Pumping	[333 $\mu$ m - 5 mm]	Zhao et al. (2015)
Yangtze Estuary (China)	4137	Subsurface (1 m)	Pumping	[32 $\mu$ m - 5 mm]	Zhao et al. (2014)
Pearl Estuary (China)	8902	Surface	5L water sampler	[50 $\mu$ m - 5 mm]	Yan et al. (2019)
Winyah Bay (USA)	30800	Surface	Sea surface microlayer collection apparatus	[63 $\mu$ m - 2 mm]	Gray et al. (2018)
Bay of Biscay	2	Subsurface (3 m)	Pumping	[250 $\mu$ m - 5 mm]	Lusher et al. (2014)
Northeastern Atlantic	2.46	Subsurface (3 m)	Pumping	[250 $\mu$ m - 5 mm]	Lusher et al. (2014)
Western Coast of Portugal	3.5	Subsurface (11 m)	Pumping	[250 $\mu$ m - 2 mm]	La Daana et al. (2017)
Bay of Biscay					

428 Microplastics have been found throughout the water column of the lower Adour Estuary, for  
 429 nearly each river discharge condition and tidal stage. Highest concentrations close to the river  
 430 bed demonstrated the importance of estimating the microplastics abundance throughout the water  
 431 column in estuaries. To limit microplastics studies to an estimation of surface abundance may  
 432 therefore lead to serious underestimation of the plastics contamination and fluxes. For instance,  
 433 simple estimates of daily fluxes as the product of the mean concentration with the river discharge  
 434 led to values of around 7 and 110 million microplastic particles exported each day toward the ocean  
 435 for low and high discharge conditions, respectively. The assumption that the total daily flux can  
 436 be approximated by the surface layer flux captured by the Manta net would lead to values about  
 437 two orders of magnitude lower, i.e. respectively to 0.07 and 1 million microplastics. It should be  
 438 additionally emphasized that a fine estimation of exported fluxes in a salt-wedge estuary would  
 439 require higher resolution and extension in the sampling protocol, allowing better characterization  
 440 of the variation of contamination in time and space in the presence of time-dependent density  
 441 stratification and its associated two-layer flow. The tidal oscillations of the estuarine waters and  
 442 the vertical structure of the current, with opposite flows during the salt-wedge passage, require an  
 443 extensive characterization of the concentration and current profiles throughout the tidal cycle to  
 444 provide relevant estimations of exported fluxes.

#### 445 4.2. *Influence of microplastics properties on their dispersion*

446 The present study has shown that the distribution of the different types of microplastics through  
447 the water column is not homogeneous. This could be due to different sources, dispersion patterns  
448 and residence times. The predominance of films and fragments in the Adour Estuary over other  
449 kinds of shapes (fibers, spheres and other) suggests that microplastics are of a secondary source (i.e.  
450 decomposition of larger items) rather than direct inputs of industrialized pellets or microspheres.  
451 Fibers represented a moderate contribution to the Adour Estuary contamination. However, fibers  
452 were predominant in sub-surface waters and in the beach sediments of the Bay of Biscay (Lusher  
453 et al., 2014; Masiá et al., 2019). This may suggest that heavier microplastics may be retained in  
454 the estuary or adjacent beaches, while fibers are able to easily flow offshore. Fibers can also have  
455 marine-based sources, i.e. fishing activities.

456 Simulations confirmed that microplastics properties play an important role with regard to  
457 the abundance and distribution of microplastics in estuaries, as well as on the flushing capacity.  
458 Neutrally-buoyant microplastics spread throughout the water column, while heavier microplastics  
459 are contained in the lower part of the water column. As a result, neutrally-buoyant microplastics  
460 are more easily flushed than heavier ones. Heavy particles are trapped inside the estuary and are  
461 therefore prone to accumulation. Field sampling revealed that near-bottom particles tend to be  
462 finer than surface ones. The hypothesis can be proposed that heavy particles trapped in the estuary  
463 are exposed to longer residence time and therefore increased degradation and fragmentation. This  
464 may partly explain why bottom microplastics sampled in the field are finer than those retrieved in  
465 the surface layer. Further density and settling velocity analysis should be performed to confirm this  
466 assumption. Overall, the numerical results confirm that all microplastics can not be considered as  
467 having the same behaviour. Three typical types of particles have been tested by the present sim-  
468 ulations in order to provide clear discrimination between dispersion patterns. The range of tested  
469 particles will be extended in the future, including in particular the particle properties extracted  
470 from the field samplings.

#### 471 4.3. *Influence of the salt-wedge dynamics on microplastics dispersion*

472 Observations and simulation results have shown that salt-wedge structure and river flow also  
473 impacts the flushing capacity and the abundance of microplastics. Observations revealed the pres-  
474 ence of concentration peaks during the tidal cycles, which can be attributed to bottom particle  
475 resuspension and/or damping of turbulent mixing by density stratification at the arrival of the  
476 salt-wedge. Simulation results confirmed that turbulence damping by density stratification induces  
477 sinking of negatively buoyant microplastics, resulting in an accumulation at the bottom of the water  
478 column. Similar features were observed in the Ebro Estuary by Simon-Sánchez et al. (2019). In  
479 estuaries where the salt-wedge structure is quasi static, the salinity front acts as a barrier for dense  
480 plastic material transported as bed load (Acha et al., 2003). As the Adour estuary demonstrated  
481 a quasi-static salt-wedge structure at neap tide during dry season, we could expect similar mech-  
482 anisms to take place under such conditions but with a total shift to another transport regime in  
483 different discharge and tide conditions (Defontaine et al., 2019). Therefore, the understanding and  
484 prediction of the salt-wedge dynamics is of major importance in the management of plastics pol-  
485 lution (Vermeiren et al., 2016) and merits further dedicated high-resolution studies. Microplastics  
486 dynamics is also driven by the riverine forcing. Observations of higher microplastics concentrations

487 for higher river discharge are here only based on two contrasted cases. The observed trends need  
488 to be confirmed by more comprehensive sampling in wider ranges of conditions. However, these  
489 observations are in line with existing observations of a positive correlation between river discharge  
490 and abundance of microplastics (Lima et al., 2014, 2015; Rodrigues et al., 2019), associating the  
491 abundance increase with higher land and city drainage during flood events. Simulations showed  
492 that stronger river flow is also responsible for increased flushing capacity of the estuary. This is due  
493 to stronger ebbing currents and associated turbulence being able to transport more particles in sus-  
494 pension out of the estuary. Combining high discharge, higher contamination and enhanced flushing  
495 capacity, the strong flood events are then expected to be a major contributor to the contamination  
496 of coastal and oceanic waters, and should therefore be monitored accordingly.

#### 497 *4.4. Simulation hypothesis and limitations*

498 A series of numerical simulations have been performed to provide further insight on the mi-  
499 croplastics dispersion processes in the Adour Estuary. Microplastics were treated as an Eulerian  
500 concentration field assuming that particle size and flow regime ensured that the particles closely  
501 follow the local flow. This approach remains consistent as long as the Stokes number of the par-  
502 ticle, i.e. the ratio between the particle relaxation time scale to the local turbulence time scale,  
503 remains small and as long as the particle concentration remains small enough to neglect interactions  
504 between particles, which is generally the case for microplastics in open marine waters. Therefore  
505 the microplastics can be simulated as a passive tracer by solving an advection-diffusion equation  
506 for the concentration including a settling velocity, the only difference with natural sediment being  
507 lower density and settling velocity for most polymer particles. Several recent works support this ap-  
508 proach by demonstrating significant correlation between microplastics and fine sediment (Rodrigues  
509 et al., 2019; Vianello et al., 2013). Both are affected by similar transport, sinking and accumulation  
510 mechanisms (Browne et al., 2010; Rodrigues et al., 2019). Microplastics may also be impacted by  
511 aggregation mechanisms similar to those affecting fine sediments, as a result of interaction with  
512 seawater and degradation mechanisms (Besseling et al., 2017; Long et al., 2015).

513 Note that, for the sake of simplicity, the turbulent diffusion for microplastics in the present  
514 numerical simulations was based on the assumptions of a turbulent Schmidt number equal to 1:  
515 microplastics and momentum are expected to diffuse at a similar rate, with a diffusion coefficient  
516 computed by the turbulence model. The current knowledge of microplastics diffusion in a tur-  
517 bulent, and possibly stratified, flow field remains very limited. Recent high-resolution laboratory  
518 measurements suggested that microplastics turbulent Schmidt numbers can significantly differ from  
519 1 (Poulain-Zarcos et al., 2020). Such research effort should be strongly fostered and extended to a  
520 wide range of real-world microplastics in order to improve the prediction performance of circulation  
521 models.

522 Numerical models are powerful tools and they usefully complement in-situ experimentations.  
523 To provide a better insight into the dynamics of microplastics contamination throughout the es-  
524 tuarine hydrosystem, simulations using more realistic configurations, including time-resolved river  
525 discharge for flood events, microplastic inputs at real sewage plant locations and/or diffuse runoff  
526 contamination will be performed. To that end, a major effort should be engaged to better monitor  
527 the microplastics inputs in the estuarine system, including incoming fluxes from each tributary,  
528 wastewater discharges and coastal waters contamination in wider ranges of conditions. It remains a

529 considerable challenge given the difficulties of operating in such contexts. The role of particle prop-  
530 erties such as shape, size, density, and settling velocity also deserves further examination. For more  
531 realistic simulations, properties of microplastics collected during the field campaign should be deter-  
532 mined in the laboratory and considered in the simulations. Nevertheless, such properties are known  
533 to be variable and time-dependent under the action of biofouling, aggregation and fragmentation  
534 (Chubarenko et al., 2018; Vermeiren et al., 2016; Wright et al., 2013). In particular, understanding  
535 and predicting the effect of biofouling on microplastics dispersion in a time-dependent salt-wedge  
536 estuary remains a stiff challenge, as the growth and decay of biofilms and the related modifications  
537 of settling velocity are intrinsically linked to the light exposure, temperature and salinity conditions  
538 (Kooi et al., 2017) which all show strong variations at various time and space scales throughout  
539 the estuarine system. Constant settling velocity was a first step for the present study and more  
540 complex dynamic properties can be introduced in the model in a future study. In addition, it should  
541 be borne in mind that no wind effect was considered in the present simulations due to its *a priori*  
542 weaker influence on the inner estuary dynamics compared to tide and discharge, in relation with  
543 an overall weak wind forcing and short fetch in the considered section of the Adour Estuary. Wind  
544 stress at the free surface is expected to add turbulence mixing near the surface (Kukulka et al.,  
545 2012) and direct stress on floating particles (Forsberg et al., 2020). These effects will be explored  
546 in further studies once the specific roles played by the two main drivers, namely tide and discharge,  
547 have been well assessed.

548 As a final note, the present study leads us to emphasize the need for further research on the  
549 complementarity and the confrontation between field sampling and numerical modelling in mi-  
550 croplastics dispersion. Field sampling is and will remain the central tool to estimate microplastics  
551 contamination. However, the cost of field sampling, both in terms of field operations and subsequent  
552 laboratory analysis, is so heavy that a comprehensive 3D time-resolved and long-term analysis of  
553 a complex and dynamic hydrosystem such as a salt-wedge estuary will remain out of reach using  
554 conventional sampling technologies. Field sampling should therefore be considered as providing  
555 snapshots of the local contamination, without any historical and spatial knowledge of microplas-  
556 tics dispersion. On the other hand, Eulerian numerical simulations are a powerful tool to provide  
557 insight on the spatial and temporal patterns of change in contamination and are therefore a useful  
558 complement to field sampling. The validity of the numerical results relies on the quality of the sim-  
559 ulated hydrodynamics (Defontaine et al., 2018) and on the assumption that microplastics can be  
560 treated as an Eulerian concentration field, as discussed above. Direct comparisons between model  
561 results and field measurements would require total control of the initial and boundary conditions  
562 within the model, with a complete knowledge of the microplastics contamination levels and particle  
563 features at the initiation of the simulations and from each potential microplastics input during  
564 the simulation. Further research work will be dedicated to this ambitious challenge, based on the  
565 fundamental knowledge gained with the present study.

## 566 5. Conclusion

567 The present study provided a first characterization of microplastics pollution in the Adour Es-  
568 tuary which is a major tributary of the southeastern Bay of Biscay. Field samplings confirmed,  
569 as for many other urban estuaries, persistent microplastic pollution. Mean abundance was esti-  
570 mated at  $1.13 \text{ part}/m^3$ , with maximum values reaching  $3.88 \text{ part}/m^3$  at the bottom of the water

571 column. Microplastics were found from the surface to the near-bottom layer, emphasizing the need  
572 to sample the entire water column to estimate relevant contamination levels and fluxes. To focus  
573 only on the surface concentrations could lead to underestimation of pollution levels. Five types  
574 of microplastics were identified, in which films and fragments were the most abundant. The mi-  
575 croplastics concentration was observed to be higher in high discharge conditions, leading to much  
576 higher total flux.

577 Numerical modelling showed that both local time-dependent and density-varying hydrodynamic  
578 conditions and microplastics properties have a determining influence on the particle dispersion,  
579 resulting in high spatial and temporal variability of abundance and distribution. The main trend was  
580 that neutrally-buoyant microplastics were easily flushed out while heavier particles were prone to  
581 be trapped in the estuary, in particular during low discharge conditions. The higher concentrations  
582 of microplastics as well as the higher proportion of fine microplastics found in the near bottom layer  
583 suggest that estuaries could be a sink of microplastics.

#### 584 **Acknowledgements**

585 This study was sponsored by the MIDYNET project (EC2CO/CNRS) and the BIGCEES project  
586 (E2S UPPA). We are grateful to the port of Bayonne for the support with the sampling.

587 Abbasi, S., Soltani, N., Keshavarzi, B., Moore, F., Turner, A., Hassanaghaei, M., 2018. Microplastics  
588 in different tissues of fish and prawn from the musa estuary, persian gulf. *Chemosphere* 205, 80–87.

589 Acha, E. M., Mianzan, H. W., Iribarne, O., Gagliardini, D. A., Lasta, C., Daleo, P., 2003. The  
590 role of the rio de la plata bottom salinity front in accumulating debris. *Marine Pollution Bulletin*  
591 46 (2), 197–202.

592 Alvim, C. B., Mendoza-Roca, J., Bes-Piá, A., 2020. Wastewater treatment plant as microplastics  
593 release source—quantification and identification techniques. *Journal of environmental management*  
594 255, 109739.

595 Andrady, A. L., 2011. Microplastics in the marine environment. *Marine pollution bulletin* 62 (8),  
596 1596–1605.

597 Bakir, A., Rowland, S. J., Thompson, R. C., 2014. Transport of persistent organic pollutants by  
598 microplastics in estuarine conditions. *Estuarine, Coastal and Shelf Science* 140, 14–21.

599 Barboza, L. G. A., Gimenez, B. C. G., 2015. Microplastics in the marine environment: current  
600 trends and future perspectives. *Marine pollution bulletin* 97 (1-2), 5–12.

601 Bellafont, F., Morichon, D., Roeber, V., André, G., Abadie, S., 2018. Infragravity period oscillations  
602 in a channel harbor near a river mouth. *Coastal Engineering Proceedings* 1 (36), 8.

603 Besseling, E., Quik, J. T., Sun, M., Koelmans, A. A., 2017. Fate of nano-and microplastic in  
604 freshwater systems: A modeling study. *Environmental Pollution* 220, 540–548.

605 Boucher, J., Friot, D., 2017. Primary microplastics in the oceans: a global evaluation of sources.  
606 IUCN Gland, Switzerland.

- 607 Brennecke, D., Duarte, B., Paiva, F., Caçador, I., Canning-Clode, J., 2016. Microplastics as vector  
608 for heavy metal contamination from the marine environment. *Estuarine, Coastal and Shelf Science*  
609 178, 189–195.
- 610 Browne, M. A., Crump, P., Niven, S. J., Teuten, E., Tonkin, A., Galloway, T., Thompson, R., 2011.  
611 Accumulation of microplastic on shorelines worldwide: sources and sinks. *Environmental science*  
612 & technology 45 (21), 9175–9179.
- 613 Browne, M. A., Dissanayake, A., Galloway, T. S., Lowe, D. M., Thompson, R. C., 2008. Ingested  
614 microscopic plastic translocates to the circulatory system of the mussel, *mytilus edulis* (l.). *En-*  
615 *vironmental science & technology* 42 (13), 5026–5031.
- 616 Browne, M. A., Galloway, T. S., Thompson, R. C., 2010. Spatial patterns of plastic debris along  
617 estuarine shorelines. *Environmental Science & Technology* 44 (9), 3404–3409.
- 618 Burchard, H., Schuttelaars, H., Ralston, D., 2018. Sediment trapping in estuaries. *Annual Review*  
619 *of Marine Science* 10 (10.1146/annurev-marine-010816-060535), 371–395.
- 620 Cadiou, J.-F., Gerigny, O., Koren, Š., Zeri, C., Kaberi, H., Alomar, C., Panti, C., Fossi, M.,  
621 Adamopoulou, A., Digka, N., et al., 2020. Lessons learned from an intercalibration exercise on  
622 the quantification and characterisation of microplastic particles in sediment and water samples.  
623 *Marine Pollution Bulletin* 154, 111097.
- 624 Chubarenko, I., Esiukova, E., Bagaev, A., Isachenko, I., Demchenko, N., Zobkov, M., Efimova, I.,  
625 Bagaeva, M., Khatmullina, L., 2018. Behavior of microplastics in coastal zones. In: *Microplastic*  
626 *Contamination in Aquatic Environments*. Elsevier, Ch. 6, pp. 175–223.
- 627 Collignon, A., Hecq, J.-H., Galgani, F., Collard, F., Goffart, A., 2014. Annual variation in neustonic  
628 micro-and meso-plastic particles and zooplankton in the bay of calvi (mediterranean-corsica).  
629 *Marine Pollution Bulletin* 79 (1-2), 293–298.
- 630 Covernton, G. A., Pearce, C. M., Gurney-Smith, H. J., Chastain, S. G., Ross, P. S., Dower, J. F.,  
631 Dudas, S. E., 2019. Size and shape matter: A preliminary analysis of microplastic sampling  
632 technique in seawater studies with implications for ecological risk assessment. *Science of The*  
633 *Total Environment* 667, 124–132.
- 634 Crawford, C., Quinn, B., 2017. Microplastics, standardisation and spatial distribution. In: *Mi-*  
635 *croplastic Pollutants*. Elsevier, Ch. 5, pp. 101–130.
- 636 Cressey, D., 2016. Bottles, bags, ropes and toothbrushes: the struggle to track ocean plastics.  
637 *Nature News* 536 (7616), 263.
- 638 Cutroneo, L., Reboa, A., Besio, G., Borgogno, F., Canesi, L., Canuto, S., Dara, M., Enrile, F.,  
639 Forioso, I., Greco, G., et al., 2020. Microplastics in seawater: sampling strategies, laboratory  
640 methodologies, and identification techniques applied to port environment. *Environmental Science*  
641 *and Pollution Research*, 1–15.
- 642 Declerck, A., Delpy, M., Rubio, A., Ferrer, L., Basurko, O., Mader, J., Louzao, M., 2019. Transport  
643 of floating marine litter in the coastal area of the south-eastern bay of biscay: A lagrangian

- 644 approach using modelling and observations. *Journal of Operational Oceanography* 12 (sup2),  
645 S111–S125.
- 646 Defontaine, S., 2019. Saline structure, circulation and suspended sediment transport in a channelized  
647 salt-wedge estuary : the adour river estuary. Ph.D. thesis, Universite de Pau et des pays de  
648 l'Adour.
- 649 Defontaine, S., Morichon, D., Sous, D., Monperrus, M., 2018. A combined numerical/experimental  
650 approach to understand stratification and mixing processes in the adour estuary. In: XVIIth  
651 International Symposium on Oceanography of the Bay of Biscay (ISOBAY 16). Anglet, France.
- 652 Defontaine, S., Sous, D., Morichon, D., Verney, R., Monperrus, M., 2019. Hydrodynamics and spm  
653 transport in an engineered tidal estuary: the adour river (france). *Estuarine, Coastal and Shelf  
654 Science* 231, 106445.
- 655 DiBenedetto, M. H., Ouellette, N. T., Koseff, J. R., 2018. Transport of anisotropic particles under  
656 waves. *Journal of Fluid Mechanics* 837, 320–340.
- 657 do Sul, J. A. I., Costa, M. F., 2014. The present and future of microplastic pollution in the marine  
658 environment. *Environmental pollution* 185, 352–364.
- 659 Dris, R., Gasperi, J., Tassin, B., 2018. Sources and fate of microplastics in urban areas: a focus on  
660 paris megacity. In: *Freshwater Microplastics*. Springer, Cham, pp. 69–83.
- 661 Fok, L., Cheung, P. K., 2015. Hong kong at the pearl river estuary: A hotspot of microplastic  
662 pollution. *Marine pollution bulletin* 99 (1-2), 112–118.
- 663 Forsberg, P., Sous, D., Stocchino, A., Chemi, R., 2020. Behaviour of plastic litter in nearshore  
664 waters: first insights from wind and wave laboratory experiments. *Marine Pollution Bulletin*.
- 665 Gago, J., Henry, M., Galgani, F., 2015. First observation on neustonic plastics in waters off nw  
666 spain (spring 2013 and 2014). *Marine environmental research* 111, 27–33.
- 667 Galgani, F., Fleet, D., Van Franeker, J., Katsanevakis, S., Maes, T., Mouat, J., Oosterbaan, L.,  
668 Poitou, I., Hanke, G., Thompson, R., et al., 2010. Marine Strategy Framework directive-Task  
669 Group 10 Report marine litter do not cause harm to the coastal and marine environment. Report  
670 on the identification of descriptors for the Good Environmental Status of European Seas regarding  
671 marine litter under the Marine Strategy Framework Directive. Office for Official Publications of  
672 the European Communities.
- 673 Galgani, F., Leaute, J., Moguedet, P., Souplet, A., Verin, Y., Carpentier, A., Goragner, H., La-  
674 trouite, D., Andral, B., Cadiou, Y., et al., 2000. Litter on the sea floor along european coasts.  
675 *Marine pollution bulletin* 40 (6), 516–527.
- 676 Gallagher, A., Rees, A., Rowe, R., Stevens, J., Wright, P., 2016. Microplastics in the solent estuarine  
677 complex, uk: an initial assessment. *Marine Pollution Bulletin* 102 (2), 243–249.
- 678 Gray, A. D., Wertz, H., Leads, R. R., Weinstein, J. E., 2018. Microplastic in two south carolina  
679 estuaries: Occurrence, distribution, and composition. *Marine pollution bulletin* 128, 223–233.

- 680 Hervouet, J.-M., 2007. Hydrodynamics of free surface flows: modelling with the finite element  
681 method. Vol. 360. Wiley Online Library.
- 682 Hidalgo-Ruz, V., Gutow, L., Thompson, R. C., Thiel, M., 2012. Microplastics in the marine en-  
683 vironment: a review of the methods used for identification and quantification. *Environmental*  
684 *science & technology* 46 (6), 3060–3075.
- 685 Isobe, A., Kako, S., Chang, P.-H., Matsuno, T., 2009. Two-way particle-tracking model for speci-  
686 fying sources of drifting objects: application to the east china sea shelf. *Journal of Atmospheric*  
687 *and oceanic technology* 26 (8), 1672–1682.
- 688 Jalón-Rojas, I., Wang, X.-H., Fredj, E., 2019. On the importance of a three-dimensional approach  
689 for modelling the transport of neustic microplastics. *Ocean Science* 15 (3), 717–724.
- 690 Kako, S., Isobe, A., Seino, S., Kojima, A., 2010. Inverse estimation of drifting-object outflows using  
691 actual observation data. *Journal of oceanography* 66 (2), 291–297.
- 692 Khatmullina, L., Isachenko, I., 2017. Settling velocity of microplastic particles of regular shapes.  
693 *Marine pollution bulletin* 114 (2), 871–880.
- 694 Kooi, M., Nes, E. H. v., Scheffer, M., Koelmans, A. A., 2017. Ups and downs in the ocean: effects  
695 of biofouling on vertical transport of microplastics. *Environmental science & technology* 51 (14),  
696 7963–7971.
- 697 Kowalski, N., Reichardt, A. M., Waniek, J. J., 2016. Sinking rates of microplastics and potential  
698 implications of their alteration by physical, biological, and chemical factors. *Marine pollution*  
699 *bulletin* 109 (1), 310–319.
- 700 Kukulka, T., Proskurowski, G., Morét-Ferguson, S., Meyer, D., Law, K., 2012. The effect of wind  
701 mixing on the vertical distribution of buoyant plastic debris. *Geophysical Research Letters* 39 (7).
- 702 La Daana, K. K., Officer, R., Lyashevskaya, O., Thompson, R. C., O’Connor, I., 2017. Microplastic  
703 abundance, distribution and composition along a latitudinal gradient in the atlantic ocean. *Marine*  
704 *pollution bulletin* 115 (1-2), 307–314.
- 705 Law, K. L., 2017. Plastics in the marine environment. *Annual review of marine science* 9, 205–229.
- 706 Lebreton, L. C., Van Der Zwet, J., Damsteeg, J.-W., Slat, B., Andrady, A., Reisser, J., 2017. River  
707 plastic emissions to the world’s oceans. *Nature communications* 8, 15611.
- 708 Lebreton, L.-M., Greer, S., Borrero, J. C., 2012. Numerical modelling of floating debris in the  
709 world’s oceans. *Marine pollution bulletin* 64 (3), 653–661.
- 710 Lenz, R., Enders, K., Stedmon, C. A., Mackenzie, D. M., Nielsen, T. G., 2015. A critical assessment  
711 of visual identification of marine microplastic using raman spectroscopy for analysis improvement.  
712 *Marine Pollution Bulletin* 100 (1), 82–91.
- 713 Li, H.-X., Ma, L.-S., Lin, L., Ni, Z.-X., Xu, X.-R., Shi, H.-H., Yan, Y., Zheng, G.-M., Rittschof,  
714 D., 2018. Microplastics in oysters *saccostrea cucullata* along the pearl river estuary, china. *Envi-*  
715 *ronmental Pollution* 236, 619–625.

- 716 Lima, A., Barletta, M., Costa, M., 2015. Seasonal distribution and interactions between plankton  
717 and microplastics in a tropical estuary. *Estuarine, Coastal and Shelf Science* 165, 213–225.
- 718 Lima, A., Costa, M., Barletta, M., 2014. Distribution patterns of microplastics within the plankton  
719 of a tropical estuary. *Environmental Research* 132, 146–155.
- 720 Long, M., Moriceau, B., Gallinari, M., Lambert, C., Huvet, A., Raffray, J., Soudant, P., 2015.  
721 Interactions between microplastics and phytoplankton aggregates: Impact on their respective  
722 fates. *Marine Chemistry* 175, 39–46.
- 723 Lusher, A. L., Burke, A., O'Connor, I., Officer, R., 2014. Microplastic pollution in the northeast  
724 atlantic ocean: validated and opportunistic sampling. *Marine pollution bulletin* 88 (1-2), 325–333.
- 725 Mani, T., Hauk, A., Walter, U., Burkhardt-Holm, P., 2015. Microplastics profile along the rhine  
726 river. *Scientific reports* 5 (1), 1–7.
- 727 Masiá, P., Ardura, A., Garcia-Vazquez, E., 2019. Microplastics in special protected areas for mi-  
728 gratory birds in the bay of biscay. *Marine pollution bulletin* 146, 993–1001.
- 729 McCormick, A. R., Hoellein, T. J., London, M. G., Hittie, J., Scott, J. W., Kelly, J. J., 2016.  
730 Microplastic in surface waters of urban rivers: concentration, sources, and associated bacterial  
731 assemblages. *Ecosphere* 7 (11), e01556.
- 732 Mendoza, A., Osa, J. L., Basurko, O. C., Rubio, A., Santos, M., Gago, J., Galgani, F., Peña-  
733 Rodriguez, C., 2020. Microplastics in the bay of biscay: An overview. *Marine Pollution Bulletin*  
734 153, 110996.
- 735 Murray, C. C., Maximenko, N., Lippiatt, S., 2018. The influx of marine debris from the great japan  
736 tsunami of 2011 to north american shorelines. *Marine pollution bulletin* 132, 26–32.
- 737 Naidoo, T., Glassom, D., Smit, A. J., 2015. Plastic pollution in five urban estuaries of kwazulu-natal,  
738 south africa. *Marine pollution bulletin* 101 (1), 473–480.
- 739 Neumann, D., Callies, U., Matthies, M., 2014. Marine litter ensemble transport simulations in the  
740 southern north sea. *Marine pollution bulletin* 86 (1-2), 219–228.
- 741 Peng, G., Zhu, B., Yang, D., Su, L., Shi, H., Li, D., 2017. Microplastics in sediments of the  
742 changjiang estuary, china. *Environmental Pollution* 225, 283–290.
- 743 Poulain-Zarcos, M., ter Halle, A., Mercier, M., 2020. Vertical distribution of particles in upper-  
744 ocean turbulence: Laboratory modelling of plastic pollution. In: *Ocean Sciences Meeting 2020.*  
745 *AGU.*
- 746 Rezanía, S., Park, J., Din, M. F. M., Taib, S. M., Talaiekhosani, A., Yadav, K. K., Kamyab, H.,  
747 2018. Microplastics pollution in different aquatic environments and biota: A review of recent  
748 studies. *Marine pollution bulletin* 133, 191–208.
- 749 Rodrigues, S., Almeida, C. M. R., Silva, D., Cunha, J., Antunes, C., Freitas, V., Ramos, S., 2019.  
750 Microplastic contamination in an urban estuary: Abundance and distribution of microplastics  
751 and fish larvae in the douro estuary. *Science of The Total Environment* 659, 1071–1081.

- 752 Sadri, S. S., Thompson, R. C., 2014. On the quantity and composition of floating plastic debris  
753 entering and leaving the tamar estuary, southwest england. *Marine pollution bulletin* 81 (1),  
754 55–60.
- 755 Sherman, P., Van Sebille, E., 2016. Modeling marine surface microplastic transport to assess optimal  
756 removal locations. *Environmental Research Letters* 11 (1), 014006.
- 757 Simon-Sánchez, L., Grelaud, M., Garcia-Orellana, J., Ziveri, P., 2019. River deltas as hotspots of  
758 microplastic accumulation: The case study of the ebro river (nw mediterranean). *Science of the*  
759 *total environment* 687, 1186–1196.
- 760 Sous, D., Defontaine, S., Morichon, D., Bhairy, N., Lanceleur, L., Monperrus, M., 2018. Turbulence  
761 measurements in a stratified man-controlled estuary, the adour case. In: *XVith International*  
762 *Symposium on Oceanography of the Bay of Biscay (ISOBAY 16)*. Anglet, France.
- 763 Stocchino, A., De Leo, F., Besio, G., 2019. Sea waves transport of inertial micro-plastics: Mathe-  
764 matical model and applications. *Journal of Marine Science and Engineering* 7 (12), 467.
- 765 Sutton, R., Mason, S. A., Stanek, S. K., Willis-Norton, E., Wren, I. F., Box, C., 2016. Microplastic  
766 contamination in the san francisco bay, california, usa. *Marine pollution bulletin* 109 (1), 230–235.
- 767 Thompson, R. C., Olsen, Y., Mitchell, R. P., Davis, A., Rowland, S. J., John, A. W., McGonigle,  
768 D., Russell, A. E., 2004. Lost at sea: where is all the plastic? *Science* 304 (5672), 838–838.
- 769 van Sebille, E., England, M. H., Froyland, G., 2012. Origin, dynamics and evolution of ocean  
770 garbage patches from observed surface drifters. *Environmental Research Letters* 7 (4), 044040.
- 771 Vermeiren, P., Muñoz, C. C., Ikejima, K., 2016. Sources and sinks of plastic debris in estuaries: a  
772 conceptual model integrating biological, physical and chemical distribution mechanisms. *Marine*  
773 *pollution bulletin* 113 (1-2), 7–16.
- 774 Vianello, A., Boldrin, A., Guerriero, P., Moschino, V., Rella, R., Sturaro, A., Da Ros, L., 2013.  
775 Microplastic particles in sediments of lagoon of venice, italy: First observations on occurrence,  
776 spatial patterns and identification. *Estuarine, Coastal and Shelf Science* 130, 54–61.
- 777 Willis, K. A., Eriksen, R., Wilcox, C., Hardesty, B. D., 2017. Microplastic distribution at different  
778 sediment depths in an urban estuary. *Frontiers in Marine Science* 4, 419.
- 779 Wright, S. L., Thompson, R. C., Galloway, T. S., 2013. The physical impacts of microplastics on  
780 marine organisms: a review. *Environmental pollution* 178, 483–492.
- 781 Xanthos, D., Walker, T. R., 2017. International policies to reduce plastic marine pollution from  
782 single-use plastics (plastic bags and microbeads): a review. *Marine pollution bulletin* 118 (1-2),  
783 17–26.
- 784 Xu, P., Peng, G., Su, L., Gao, Y., Gao, L., Li, D., 2018. Microplastic risk assessment in surface  
785 waters: A case study in the changjiang estuary, china. *Marine Pollution Bulletin* 133, 647–654.
- 786 Yan, M., Nie, H., Xu, K., He, Y., Hu, Y., Huang, Y., Wang, J., 2019. Microplastic abundance,  
787 distribution and composition in the pearl river along guangzhou city and pearl river estuary,  
788 china. *Chemosphere* 217, 879–886.

- 789 Yonkos, L. T., Friedel, E. A., Perez-Reyes, A. C., Ghosal, S., Arthur, C. D., 2014. Microplastics  
790 in four estuarine rivers in the chesapeake bay, usa. *Environmental science & technology* 48 (24),  
791 14195–14202.
- 792 Zhao, S., Zhu, L., Li, D., 2015. Microplastic in three urban estuaries, china. *Environmental Pollution*  
793 206, 597–604.
- 794 Zhao, S., Zhu, L., Wang, T., Li, D., 2014. Suspended microplastics in the surface water of the  
795 yangtze estuary system, china: first observations on occurrence, distribution. *Marine pollution*  
796 *bulletin* 86 (1-2), 562–568.